
Improved Detection and Localization of Lower Gastrointestinal Tract Hemorrhage by Subtraction Scintigraphy: Phantom Analysis

Geoffrey M. Currie, CNMT¹, Philip A. Towers², and Janelle M. Wheat¹

¹*School of Clinical Sciences, Charles Sturt University, Wagga Wagga, New South Wales, Australia;* and ²*School of Biomedical Sciences, Charles Sturt University, Wagga Wagga, New South Wales, Australia*

Acute lower gastrointestinal tract hemorrhage (LGIH) has significant morbidity and mortality outcomes. Although several causes of LGIH can be life threatening, most can be effectively treated; therefore, early detection and accurate localization of bleeding sites are critical for successful patient management. **Methods:** This study was a phantom experimental study with a repeated-measures design. The minimum detectable bleeding rate, the minimum detectable bleed volume, the sensitivity for detection, and the time required for detection were determined and compared for conventional scintigraphy (CS) and 3 experimental techniques: reference subtraction scintigraphy (RSS), sequential subtraction scintigraphy (SSS), and alternate sequential subtraction scintigraphy (ASSS). **Results:** The minimum detectable bleeding rates within the first hour were 0.05 mL·min⁻¹ for CS and RSS, 0.1 mL·min⁻¹ for ASSS, and 0.5 mL·min⁻¹ for SSS. This study demonstrated minimum detectable bleed volumes of 2.2 mL for CS, 2.3 mL for RSS, 5 mL for ASSS, and 5 mL for SSS stratified to a “definitely present” certainty. No statistically significant difference was noted in the mean time to detection between CS and the subtraction techniques. Receiver-operating-characteristic analysis indicated that combining CS and RSS improved test performance and increased overall sensitivity to 75% from 68.3% for CS and 71.7% for RSS. **Conclusion:** Supplementing conventional datasets with RSS and ASSS may provide a useful tool that combines the advantages offered for lesion detectability by a high-contrast ^{99m}Tc-sulfur colloid study with the window of opportunity offered by ^{99m}Tc-labeled red blood cell scanning.

Key Words: bowel hemorrhage; gastrointestinal tract bleed; subtraction scintigraphy; localization; LGIH

J Nucl Med Technol 2006; 34:160–168

Diagnostic evaluation of acute lower gastrointestinal tract hemorrhage (LGIH) is significantly more difficult than that of upper gastrointestinal tract hemorrhage (1,2). Several features contribute to the diagnostic conundrum

Received Aug. 26, 2005; revision accepted Nov. 21, 2005.
For correspondence or reprints contact: Geoffrey M. Currie, CNMT, School of Clinical Sciences, Locked Bag 588, Charles Sturt University, Wagga Wagga, New South Wales 2678, Australia.
E-mail: gcurrie@csu.edu.au
COPYRIGHT © 2006 by the Society of Nuclear Medicine Technology, Inc.

for acute LGIH (3): the origin of bleeding may be anywhere in the gastrointestinal tract, bleeding is frequently intermittent, evidence of active bleeding may not be obvious until after bleeding has ceased, and emergency surgery may be required for both a specific diagnosis and localization of the bleeding site.

Furthermore, the value of an accurate diagnostic evaluation may vary among patients because the recurrence of bleeding after therapy is common and there is no consensus on appropriate patient management (3). Despite these problems, accurate localization of the site of bleeding is crucial for treatment and patient management (4,5).

There are currently 3 main options for the detection and localization of LGIH sites: colonoscopy, angiography, and ^{99m}Tc-labeled red blood cell (RBC) scintigraphy (6–8). Although diagnostic evaluation of acute LGIH has improved significantly over the last 25 y, procedures are not universally successful (9). There is currently no gold standard for evaluating acute LGIH because of the intermittent nature of the bleeding (1,5,10). Despite advances in diagnostic evaluation, a bleeding site is not identified for 8%–12% of patients with acute LGIH (11).

Currently, only about 10% of patients presenting with LGIH are evaluated by nuclear medicine scintigraphy (1,12). Improving this technique to provide earlier detection and more precise localization of bleeding sites may facilitate its elevation to the leading diagnostic tool, filling the void left in the absence of a recognized gold standard.

Subtraction scintigraphy has been used in nuclear medicine for parathyroid imaging to delineate thyroid tissue from parathyroid tissue (13–15) and for the assessment of prosthetic joints to differentiate infection from marrow compaction after surgery (13). An underused application of subtraction scintigraphy is the evaluation of acute LGIH by ^{99m}Tc-labeled RBC scintigraphy.

Several authors have documented the use of subtraction scintigraphy to improve image contrast in ^{99m}Tc-labeled RBC evaluation of acute LGIH (16,17). Either the first frame acquired or a summation of all images with normalization for count density is used to represent a background image and is subsequently subtracted from each

individual image (16,17). Gore et al. (18) described the use of image subtraction to improve the localization of a bleeding site. Kouris et al. (19) used subtraction scintigraphy to overcome interpretation difficulties associated with high background activity in ^{99m}Tc -labeled RBC studies, liver and spleen activity in ^{99m}Tc -sulfur colloid studies, and bladder and kidney activity in ^{99m}Tc -diethylenetriamine-pentaacetic acid studies.

In essence, subtracting a nominal “mask” or reference image (generally an early image in the dynamic sequence) from all subsequent images provides a mechanism to view only the information contributed by accumulated bleeding. This technique allows the removal of potential sources of false-positive results or the removal of superimposed structures (e.g., liver). The reference method has been referred to as reference subtraction scintigraphy (RSS). There are, however, several assumptions that are not necessarily met for patient data:

- There should be minimal patient motion between the reference frame and any image to be subtracted. With the first frame as the reference frame, the patient must be motionless for the entire acquisition (usually 60 min).
- The biodistribution of the radiopharmaceutical should be stable between the reference frame and any image to be subtracted. Normalization of count density can accommodate physical decay of the radionuclide; however, altered biodistribution (e.g., excretion, label breakdown) may be present in image subtraction.

Also to be considered is the degree of change that the selected sampling interval is capable of demonstrating.

Sequential subtraction scintigraphy (SSS) has also been described to improve the detection and localization of LGIH (20–22). This technique involves the subtraction of each image from the next image in the sequence, thus leaving only that which has changed in the interval between images (20–22). The technique was first described by Kouris et al. (19) with 5-min images to more accurately delineate fresh bleeding. Assumptions and limitations sim-

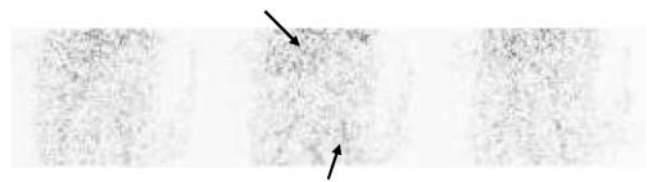


FIGURE 1. Sequential subtraction images of normal study. Liver (top arrow) and large vessel (bottom arrow) activities can be faintly visualized.

ilar to those for RSS apply to SSS; however, the impact of effects varies:

- Patient motion is still problematic; however, only subtracted images for which there is evidence of motion between consecutive images will be affected. For example, motion in frame 6 will produce artifacts only in the 2 subtracted images produced with frame 6.
- Variations in the biodistribution of the radiopharmaceutical, even in the presence of label breakdown, should be minimal in the period between consecutive images and therefore have a minimal negative impact on the subtracted dataset.
- Similarly, normalization is not generally required because the amount of radioactive decay between consecutive images is negligible.
- The sampling frame is crucial. Also to be considered is the statistical certainty associated with count density as the time per frame becomes shorter, particularly for lower bleeding rates. The critical volume for bleed detection must be considered while one is optimizing the interval for minimal decay, minimal alterations to biodistribution, and, most importantly, minimal dispersion of blood through the bowel lumen within a single sampling frame.

SSS was tested clinically by the first author in 1998 with 1-min sampling intervals to remove the high background activity and superimposed activity of high-count organs, such as the liver (Fig. 1). This technique showed potential

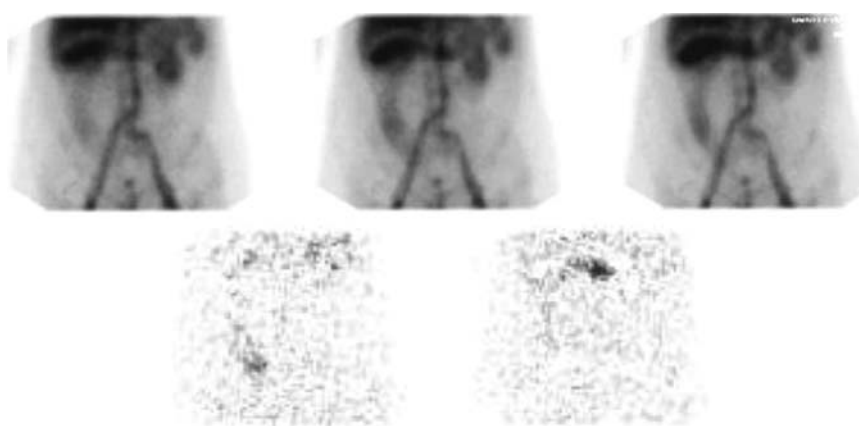


FIGURE 2. (Top) Conventional ^{99m}Tc -labeled RBC scintigrams demonstrating diffuse ascending colon accumulation of radiopharmaceutical without identification of specific bleeding site. Focal accumulation of radiopharmaceutical in transverse colon may suggest bleeding origin with rapid retrograde movement of blood into ascending colon. (Bottom) SSS demonstrates proximal ascending colon bleeding source that precedes the transverse colon accumulation.

for earlier detection and improved localization of bleeding sites in acute LGIH (Fig. 2).

During ^{99m}Tc -labeled RBC scintigraphy, activity at the bleeding site will steadily increase while active bleeding persists. This technique assumes the extravasation of ^{99m}Tc -labeled RBCs in a continuous manner while background activity remains relatively unchanged. It also neglects the impact of retrograde and antegrade movement of extravasated blood away from the bleeding site. Subtracting sequential images should allow the elimination of background activity, providing images of the extravasated blood with high target-to-background activity. In short, a dataset that theoretically offers the advantages of both a conventional ^{99m}Tc -sulfur colloid study and ^{99m}Tc -labeled RBC scintigraphy is produced. An alternative approach has been postulated from this research: alternate SSS (ASSS).

The question considered in this research is whether subtraction scintigraphy provides earlier detection than, more accurate localization than, and improved sensitivity over conventional scintigraphic imaging for simulated LGIH in a phantom model. The aim of this investigation was to evaluate, in comparison with conventional scintigraphy (CS) and in a phantom model, the abilities of 3 subtraction scintigraphy methods (RSS, SSS, and ASSS) to decrease the minimum detectable bleeding rate, increase the sensitivity for detection of LGIH, and allow earlier detection of bleeding sites.

MATERIALS AND METHODS

Study Design

This phantom study was an experimental study with a repeated-measures design (within-subject design). This design allowed evaluation of the response variables by manipulation of the explanatory variables within a single acquisition dataset; therefore, a single dataset acted as both the control group (CS) and the 3 experimental groups (RSS, SSS, and ASSS). The major disadvantage associated with this design is in the observer interpretation: the order or sequence of observations may confound the results. Consequently, all datasets for interpretation were randomized before observer interpretation. Matched control and experimental data were independent within the randomized pool. Randomization was thought to offer simplicity and superiority in controlling potential confounding in comparison with the counterbalancing method.

The response variables for this phantom study included the minimum detectable bleeding rate, the minimum detectable bleed volume, the sensitivity for detection, and the time required for detection. The explanatory variables for this phantom study were the phantom, acquisition and processing parameters, bleeding rate, bleed volume, bleed position, sampling interval, and processing method (CS, RSS, SSS, and ASSS).

Phantom Parameters

An abdominal phantom was constructed to emulate the human biodistribution of ^{99m}Tc -labeled RBCs. All calculations were based on a 740-MBq dose of ^{99m}Tc -labeled RBCs in a reference

man by use of a single-compartment model (vascular). A reference man was chosen over a reference woman only by convention; the selected characteristics were derived from the International Commission on Radiological Protection (ICRP) Report of the Task Group on Reference Man (23). Final specific concentrations of radionuclide activity for the phantom were determined on the basis of area rather than volume, as the imaging procedure was performed with a single, 2-dimensional planar projection offering no depth discrimination.

The phantom was constructed to simulate abdominal background activity, liver activity, and great-vessel activity (descending aorta and inferior vena cava [IVC]). Although these structures have a normal appearance on a gastrointestinal tract hemorrhage study with ^{99m}Tc -labeled RBC imaging, they are not the only structures offering potential false-positive and false-negative results (e.g., renal excretion). The purpose of this investigation, however, was not to evaluate performance in relation to specific causes of false-positive or false-negative findings but rather to evaluate the technique in relation to general performance with superimposed activity. The liver and IVC of the abdomen offer the most prominent accumulation of ^{99m}Tc -labeled RBCs, and the mesenteric blood volume produces relatively uniform background activity. Moreover, the liver provides an intense but uniform background for the bleed, and the IVC provides an intense background with variations in uniformity attributable to edges (i.e., a small structure on the x -axis).

Hemorrhages were simulated in several positions (Fig. 3): in a background-only area, superimposed on the liver, and superimposed on the IVC.

Bleeding was simulated by use of a Terufusion TE-331 syringe pump which, when used with the Terumno syringe, provides an accuracy of $\pm 3\%$. Breather needles (23 gauge) were used with evacuated vials to remove any pressure differentials between the vial and the atmosphere, allowing consistent and accurate infusion rates. The evacuated vial was placed in an upright position to provide a relatively contained area for the simulated bleed. Although this technique maximizes counts per pixel and therefore provides ideal conditions for early detection, it does not provide a realistic representation of a physiologic bleed, because extravasated blood generally does not remain at a focal collection point. This technique was preferred first because it allowed experimental control and second because the physiologic behavior of the bleed

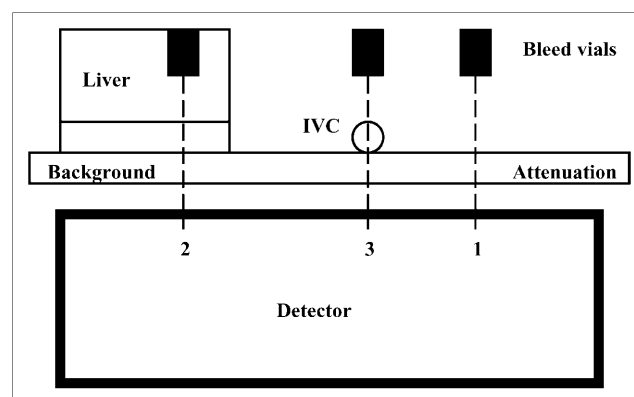


FIGURE 3. Cross section through phantom apparatus simulating bleed locations in background (1), superimposed on liver (2), and superimposed on IVC (3).

could not be adequately modeled in the phantom study. A 75-cm extension tube was primed with the radiotracer and used to connect the 60-mL syringe driven by the infusion pump to the collection vial via a 23-gauge needle.

Validation of Phantom Parameters

Before commencement of the phantom experiments, the theoretic specific concentrations of radionuclide activities were tested against the clinical model. The abdominal phantom was prepared and, excluding the hemorrhages themselves, was imaged with a 1-min dynamic acquisition for 10 min with a 128×128 acquisition matrix. Regions of interest (ROIs) were drawn on the first 1-min frame to include background, liver, and blood vessels, and the counts per pixel for the 3 regions were determined.

Five clinical RBC studies of the abdomen also were used. The clinical studies were obtained with in vitro RBC labeling, 1-min dynamic imaging, and a 128×128 acquisition matrix. ROIs were drawn on the first blood-pool frame to include background, liver, and major blood vessels, and the counts per pixel for each were determined. Comparison was made between the phantom and clinical studies for relationships among the counts per pixel for the ROIs (liver-to-background, IVC-to-background, and liver-to-IVC ratios).

Although this analysis was not expected to provide definitive statistical evidence that the phantom parameters represent the mean statistics of a large group of patients, it was designed to provide confirmation that both the counts per pixel and the relationships among the count densities for the main structures are within the range expected in clinical studies. It should be noted that the model does not account for the magnitude of individual doses used clinically, gross blood loss in some patients, variable radiopharmaceutical breakdown, variable patient attenuation, possible patient morbidity (e.g., liver disease), possible patient motion, or other factors that may contribute to deviations of the phantom model from the human model.

Data Acquisition

All data were acquired with a Philips Prism 1000 single-detector γ -camera and a Philips Odyssey VP computer. Acquisition parameters for all datasets included a 128×128 matrix and a dynamic acquisition of 10 s per frame. The photopeak was centered around the 140-keV γ -emission of ^{99m}Tc with a 15% width. Data were collected in the byte mode (depth of 8) rather than the word mode (depth of 16) to accommodate the large number of frames within the acquisition computer memory. The main concern arising from the use of the byte mode was the limited number of counts per pixel able to be stored (255 vs. 65,535). Given the rapid framing rate and the sizes of individual pixels, the counts per pixel were relatively low (on the order of 100 for the maximum pixel count); therefore, pixel overflow was not problematic. Moreover, summation of the counts per pixel during reframing and matrix conversion did not result in the subsequent truncation of counts at 255 counts per pixel, thus allowing accurate representation of all data.

Datasets representing simulated bleeding infusion rates of 0.01, 0.015, 0.02, 0.05, 0.1, 0.5, 1.0, and 2 $\text{mL}\cdot\text{min}^{-1}$ were acquired with the bleeding site in the background, superimposed on the liver, and superimposed on the IVC. This procedure resulted in the production of 24 individual datasets.

Data Processing

There were 24 original datasets representing 8 different bleeding rates and 3 bleeding sites. These 24 datasets were converted from a 10-s sampling interval to 30-s, 60-s, and 5-min sampling intervals to produce (inclusive of the 10-s sampling interval) 96 individual datasets. Each of the 96 datasets was displayed conventionally without subtraction (CS), with RSS, with SSS, and with ASSS, resulting in 384 individual studies requiring subjective and semiquantitative evaluations.

For each combination of variables, a conventional dataset (CS) and 3 subtraction datasets (RSS, SSS, and ASSS) were produced for evaluation. Each study was evaluated with regard to the presence of a bleed and the frame number of first detection. For each dataset, a frame number was identified to correspond to the following: the first frame in which a bleed was definitely present, the first frame in which a bleed was probably present, the last frame in which a bleed was probably absent, and the last frame in which a bleed was definitely absent. It is clear that the last frame in which a bleed was probably absent and the first frame in which a bleed was probably present may not be contiguous. Frames between these points were considered equivocal.

Knowing the sampling interval of an individual dataset allowed determination of the time required for detection and thus the minimum bleeding volume required for detection. The time to detection and the minimum detectable bleeding volume were determined in each dataset from the first frame in which the bleed was definitely present and the first frame in which the bleed was probably present.

All studies were randomly evaluated independently by 2 experienced observers who were unaware of the other observers' results. The benefit of random evaluation was negated somewhat for the following reasons:

- Observers were aware that a bleed was expected in 1 of 3 possible locations.
- Experienced operators could easily deduce the acquisition parameters used because of the count density and the number of frames. The bleeding rate, however, remained unknown, so that observers did not know if or when to expect a bleed.
- No negative datasets were used; therefore, a false positivity rate could not immediately be calculated. However, observers were aware that some datasets would fall below the minimum detectable bleeding volume or bleeding rate.

RSS

In an acquisition with n consecutive image frames and with each individual image frame given by $F(f)$, where f equals $(1, 2, 3, \dots, n)$, any subtracted image in the sequence is given by the following equation:

$$S(f) = F(f) - F(1).$$

For example,

$$S(10) = F(10) - F(1).$$

It is clear that f cannot equal 0 and that there is no $n + 1$; therefore, only $n - 2$ subtracted frames are produced. All subtraction images used frame 1 as the baseline (Fig. 4).

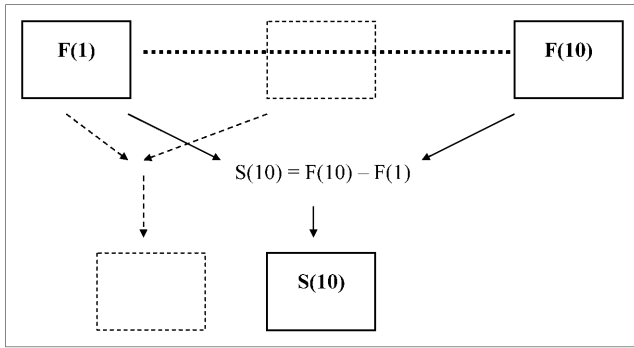


FIGURE 4. Schematic representation of RSS. Each individual frame has subtracted from it the initial reference frame.

SSS

In an acquisition with n consecutive image frames and with each individual image frame given by $F(f)$, where f equals $(1,2,3,\dots,n)$, any subtracted image in the sequence is given by the following equation:

$$S(f + 1, f) = F(f + 1) - F(f).$$

For example,

$$S(10, 9) = F(10) - F(9).$$

It is clear that f cannot equal 0 and that there is no $n + 1$; therefore, only $n - 1$ subtracted frames are produced. In theory, $f + 1$ will contain fewer counts than f because of decay, and this factor may provide a limitation for the minimum detectable bleeding volume. The subtraction method should result in the removal of temporally consistent image data, such as background, to allow better visualization of active bleeding (Fig. 5).

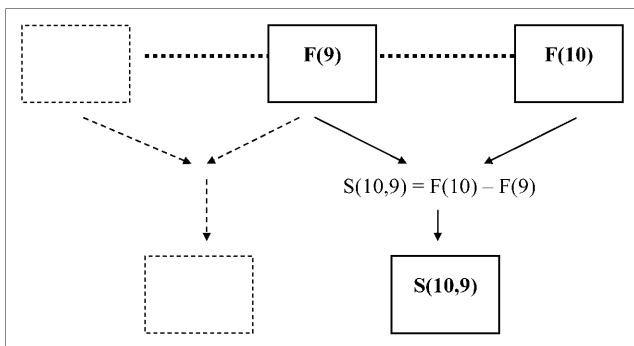


FIGURE 5. Schematic representation of SSS. Each individual frame has subtracted from it the preceding frame.

ASSS

In an acquisition with n consecutive image frames and with each individual image frame given by $F(f)$, where f equals $(1,2,3,\dots,n)$, any subtracted image in the sequence is given by the following equation:

$$S(f) = F(f + 1) - F(f - 1).$$

For example,

$$S(9) = F(10) - F(8).$$

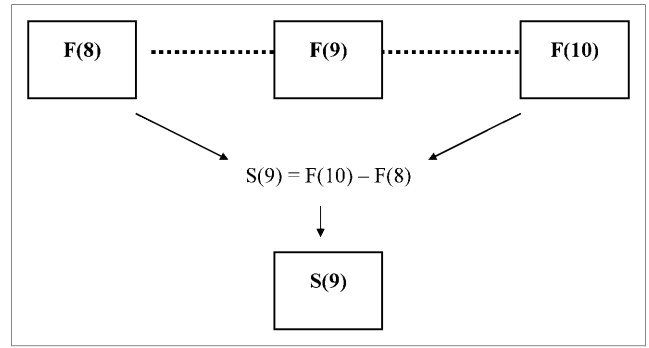


FIGURE 6. Schematic representation of ASSS. Each new frame is produced by subtraction of the preceding frame from the subsequent frame.

It is clear that f cannot equal 0 and that there is no $n + 1$; therefore, only $n - 2$ subtracted frames are produced (Fig. 6).

Statistical Analysis

Statistical significance was calculated by χ^2 analysis for nominal data and the Student t test for continuous data. The Pearson χ^2 test was used for categorical data with a normal distribution, and the G^2 likelihood ratio χ^2 test was used for categorical data without a normal distribution. The F test ANOVA was used to determine statistically significant differences within grouped data. A P value of less than 0.05 was considered significant.

Differences between independent means and proportions were calculated with a 95% confidence interval (CI). CIs without an overlap or those that did not include 0 were considered to support a statistically significant difference, whereas CIs with an overlap or those that included 0 represented differences for which chance could not be excluded as the cause. Receiver-operating-characteristic (ROC) analysis was performed with JROCFIT software version 1.0.2, developed by Dr. John Eng at Johns Hopkins University as a translation of the ROCFIT program developed by Dr. Charles Metz at the University of Chicago.

Interobserver correlation was evaluated with χ^2 analysis, and interobserver reliability was measured with the Cohen κ -coefficient. Bland-Altman analysis (24) and the matched-pairs t test were used to assess agreement between pairs (observers and processing methods).

RESULTS

Validation of Phantom Parameters

The count densities of key structures (counts per pixel) of the phantom fell within the maximum and minimum ranges determined from the clinical database (Table 1). Similarly, the ratios of count densities among the key structures for the phantom fell within the range determined from the clinical database (Table 1). Although these data do not provide conclusive evidence that the phantom parameters satisfy the distribution of the mean values determined from a large clinical database, they do provide evidence that the phantom parameters are within the clinical range.

TABLE 1

Comparison of Maximum and Minimum Counts and Ratios for Structures from Clinical Database with Those from Phantom*

Parameter	Clinical minimum–maximum (phantom)	Clinical mean (95% CI)	<i>P</i> (mean vs. phantom)
Liver counts/pixel	135.6–365.6 (212.8)	230.3 (112.7–348.0)	0.70
IVC counts/pixel	118.8–247.6 (167.2)	164.7 (96.4–233.0)	0.92
Background counts/pixel	39.8–122.0 (70.0)	72.8 (25.9–119.8)	0.87
Liver-to-IVC ratio	1.0–1.9 (1.3)	1.40 (0.95–1.86)	0.56
Liver-to-background ratio	2.6–4.8 (3.0)	3.38 (2.26–4.51)	0.40
IVC-to-background ratio	1.6–3.1 (2.4)	2.47 (1.78–3.16)	0.80

*All phantom parameters fell within clinical range.

Interobserver Agreement

Interobserver agreement was determined with respect to both the presence of a bleeding site and the time to detection. A total of 1,536 observations were made by each observer. With respect to the presence or absence of a bleeding site, the interobserver agreement was 0.988. The overall correlation of the time to detection for all 1,536 observations per observer demonstrated no statistically significant difference between matched pairs ($P = 0.586$); the correlation coefficient was 0.867. The mean difference between observer 1 and observer 2 was -0.054 min (95% CI: -0.247 to 0.139). When the data were limited to observations with substantive time entries, a stronger correlation was demonstrated between observers; the interobserver correlation coefficient was 0.944. The mean difference in time to detection between observers was 0.445 min (26.7 s), with a 95% CI of 0.037 – 0.853 and an SD of 3.63.

Minimum Detectable Bleeding Rate

The minimum detectable bleeding rates within the first hour were 0.05 mL·min⁻¹ for the 5-min sampling interval, 0.1 mL·min⁻¹ for the 30- and 60-s sampling intervals, and 0.5 mL·min⁻¹ for the 10-s sampling interval. The minimum detectable bleeding rates within the first hour were 0.05 mL·min⁻¹ for the 5-min sampling interval with CS and RSS, 0.1 mL·min⁻¹ for the 5-min sampling interval with ASSS, and 0.5 mL·min⁻¹ for the 5-min sampling interval with SSS. The minimum detectable bleeding rates within the first hour were 0.05 mL·min⁻¹ for the 5-min sampling interval in the background and the liver and 0.5 mL·min⁻¹ for the 5-min sampling in the IVC.

Time to Detection

The mean times to detection of the bleed were 16.67 min (95% CI: 13.51–19.83) for definitely present and 11.81 min (95% CI: 9.61–14.02) for probably present. The minimum times to detection were 4.8 min for definitely present and 3 min for probably present.

The mean times to detection of the bleed were 12.36 min (95% CI: 9.86–14.86) with CS and 13.17 min (95% CI: 10.91–15.42) with RSS. Consistent with the overlap of 95% CIs, no statistically significant difference was noted be-

tween the means ($P = 0.522$). The minimum times to detection were 3 min with CS and 4 min with RSS. The mean difference between datasets was 0.81 min (95% CI: -0.84 to 2.45), and the matched-pairs *t* test did not demonstrate a statistically significant difference between groups ($P = 0.332$); this finding is supported by the 95% CIs including 0.

No statistically significant difference was noted in the mean times to detection with CS (11.43 min) and SSS (10 min) ($P = 0.457$). No statistically significant difference was noted in the mean times to detection with CS (14.45 min) and ASSS (15 min) ($P = 0.333$).

Minimum Detectable Bleed Volume

The minimum detectable bleed volumes for definitely present were 2.15 mL with CS and 2.3 mL with RSS. The minimum detectable bleed volumes for probably present were 1.65 mL with CS and 1.9 mL for RSS. No statistically significant difference was noted in the minimum detectable bleed volumes between processing methods ($P = 0.79$). It is worth noting, however, that the minimum detectable bleed volumes were lower with CS than with the subtraction methods in the more uniform background and liver, whereas RSS and ASSS demonstrated lower minimum detectable bleed volumes than did CS in the IVC (SSS was the same as CS).

A statistically significant difference was noted between the mean minimum detectable bleed volumes in the background (3.00 mL; 95% CI: 0.73–5.27) and IVC (7.75 mL; 95% CI: 5.48–10.02) ($P = 0.006$). No statistically significant difference was noted between the mean minimum detectable bleed volumes in the liver (5.88 mL; 95% CI: 3.62–8.15) and IVC (7.75 mL; 95% CI: 5.48–10.02) ($P = 0.07$). No statistically significant difference was noted between the mean minimum detectable bleed volumes in the liver (5.88 mL; 95% CI: 3.62–8.15) and background (3.00 mL; 95% CI: 50.73–5.27) ($P = 0.23$).

ROC Analysis

Combining CS and RSS improved test performance from 0.891 to 0.908. That is, RSS improved the probability that CS would show more suspicious findings for a bleed in a study with a bleed than in a study without a bleed by 2%.

Both SSS and ASSS showed no increase in the area under the ROC curve, with 0.891 for each. Combining CS and RSS also increased overall sensitivity to 75% from 68.3% for CS and 71.7% for RSS (note that RSS offered higher sensitivity). Values are relative to the experimental model and have no absolute external validity.

DISCUSSION

It is clear from the data that the time to detection is delayed by lower bleeding rates and more rapid sampling intervals. However, sampling interval increases also may result in a delay in detection. These findings may seem counterintuitive, because the count density and therefore the image quality increase with sampling interval increases. The problem lies in the minimum detectable volume being satisfied early in an image frame. For example, a bleed could be detected at 6.5 min with the 30-s sampling interval but at 7 min with the 60-s sampling interval or at 10 min with the 5-min sampling interval. Bleeding would be clearly detectable at 6.5 min, but this time would coincide with the middle of a frame acquisition for the 60-s sampling interval, at the beginning of the 5-min sampling interval, and at the end of the 30-s sampling interval. The impact of this averaging effect on temporal resolution is particularly evident in a comparison of detection times for 60-s versus 5-min sampling intervals for both observers. One might assume, therefore, that there is little merit in acquiring or displaying data at 5-min intervals; however, lower bleeding rates are detected only with longer intervals (e.g., $0.05 \text{ mL}\cdot\text{min}^{-1}$). An interesting trade-off exists, therefore, between the detection of slower hemorrhages at longer sampling intervals and the early detection (more accurate localization) of more rapid hemorrhages. The solution probably lies in acquiring the data with rapid sampling and displaying the data at multiple sampling intervals (i.e., 1- and 5-min frames).

Although under ideal experimental conditions, the minimum detectable bleeding rate scintigraphically (CS and RSS) within 60 min was $0.05 \text{ mL}\cdot\text{min}^{-1}$, the external validity of this value (and even the internal validity) can be questioned. First, the earliest that a bleed at this minimum rate was definitely detected was after 40 min of bleeding. A $0.05 \text{ mL}\cdot\text{min}^{-1}$ bleed therefore would need to be both continuous for 40 min and commence within the first 20 min of a 60-min acquisition to be detected. Second, this minimum detectable bleeding rate is valid only for the high-contrast and relatively uniform scenario presented by a bleed within the mesenteric background. Even within the confines of this experimental phantom, a bleeding rate of $0.1 \text{ mL}\cdot\text{min}^{-1}$ is required to reliably detect a bleed obscured by other vascular structures (e.g., liver or IVC), notwithstanding the first limitation outlined earlier. Third, the extravasated blood volume in a clinical study may not remain focal; diffusion through the bowel lumen is likely.

A minimum detectable bleeding rate of $0.05 \text{ mL}\cdot\text{min}^{-1}$ is consistent with the rate reported by Alavi et al. (25) using $^{99\text{m}}\text{Tc}$ -sulfur colloid experimentally, the rate of $0.04 \text{ mL}\cdot\text{min}^{-1}$ reported by Thorne et al. (26) using $^{99\text{m}}\text{Tc}$ -labeled RBCs, and the rate of $0.04 \text{ mL}\cdot\text{min}^{-1}$ reported by Datz et al. (27). The minimum detectable bleeding rates with ASSS and SSS were 0.1 and $0.5 \text{ mL}\cdot\text{min}^{-1}$, respectively. These subtraction results are on the same order as those reported by Chandeysson et al. (28) using the low-background areas of a phantom to demonstrate a detectable bleeding rate of $0.2 \text{ mL}\cdot\text{min}^{-1}$. The minimum detectable bleeding rate increases with decreasing sampling interval, increases with decreasing target-to-background ratio, increases with decreasing background uniformity, and increases with subtraction scintigraphy.

Regardless of the minimum detectable bleeding rate, the minimum extravasated blood volume for the detection of acute LGIH has been reported to be 3.0–5.0 mL (29–31). Experimentally, this study demonstrated minimum detectable bleed volumes of 2.2 mL for CS, 2.3 mL for RSS, 5 mL for ASSS, and 5 mL for SSS stratified to a “definitely present” certainty. The importance of these results clinically is reflected in the statistically significant increase in the minimum detectable bleed volume between the background and the IVC ($P = 0.006$). One should, however, keep in mind that in the clinical model, a larger bleed volume would have the increased impact of rapid movement of blood through the bowel lumen, confounding such calculations.

The mean times to the detection of the bleed were 12.36 min (95% CI: 9.86–14.86) for CS and 13.17 min (95% CI: 10.91–15.42) for RSS. There was a statistically significant difference between the mean differences in times to bleed detection between CS and RSS relative to the site of the bleed ($P < 0.0001$). Hemorrhages positioned in the background and liver showed mean differences of 4.2 and 3.6 min, respectively, yet hemorrhages positioned in the IVC showed a mean difference of -7.1 min. The negative integer indicates that RSS provided more rapid detection than did CS for IVC hemorrhages.

No statistically significant differences were noted for time to detection in matched pairs between CS and both SSS and ASSS. It is worth noting that the earliest that each method can detect a bleed will be the sampling interval for CS, 2 times the sampling interval for RSS and SSS, and 3 times the sampling interval for ASSS. RSS improves the time to detection in the IVC, a result that suggests that clinically, RSS may be useful in detecting some hemorrhages not revealed by CS because of a nonuniform background, an intense background, or high-count-density structure edges (Figs. 7–9). It is also unusual that, with a consistent bleeding rate, if SSS or ASSS results were going to be positive, these methods should be effective from 10 min (frame 2 – frame 1) and 15 min (frame 3 – frame 1), respectively. Because this finding was not the observation of this study, with times to detection as high as 50 min,

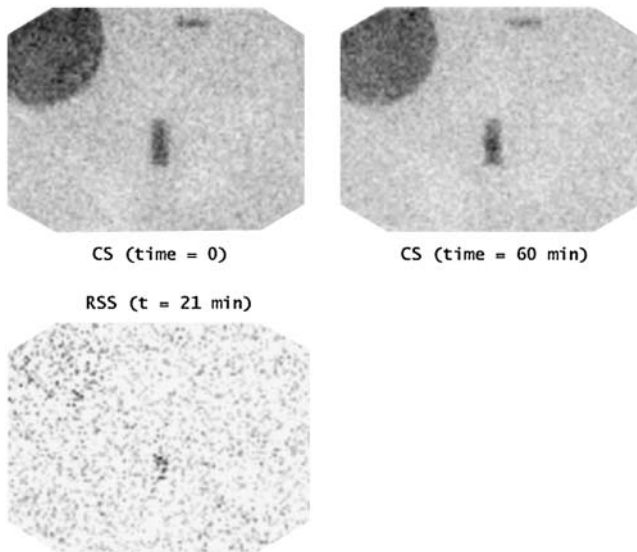


FIGURE 7. Bleed rate of $0.5 \text{ mL}\cdot\text{min}^{-1}$ with 10-s sampling interval. Interpretation with CS at 60 min is probably equivocal, especially if one were not aware of precisely where bleed was expected. However, RSS at just 21 min provides “probably present” outcome for IVC bleed position.

subtraction scintigraphy requires satisfaction of a bleed count threshold at which the minimum bleed volume required may be proportional to the presubtraction background activity.

It comes as no surprise at this point that ROC analysis indicated that CS was the superior method for the background and liver bleed positions, whereas RSS was superior for the IVC bleed position. These data are very important

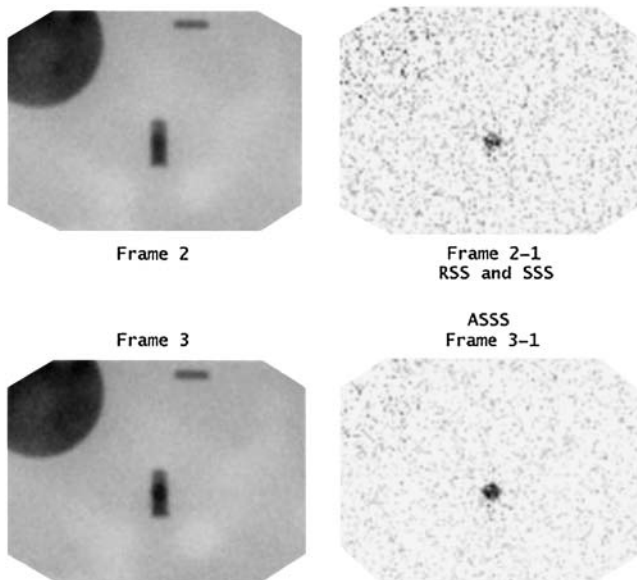


FIGURE 8. Bleed rate of $1.0 \text{ mL}\cdot\text{min}^{-1}$ with 5-min sampling interval. Lack of certainty exists for this IVC bleed position in CS frames 2 and 3 (left images). However, RSS (frame 2 – frame 1) and ASSS (frame 3 – frame 1) provide “definitely present” outcome. In this example, RSS and SSS produce the same subtraction image.

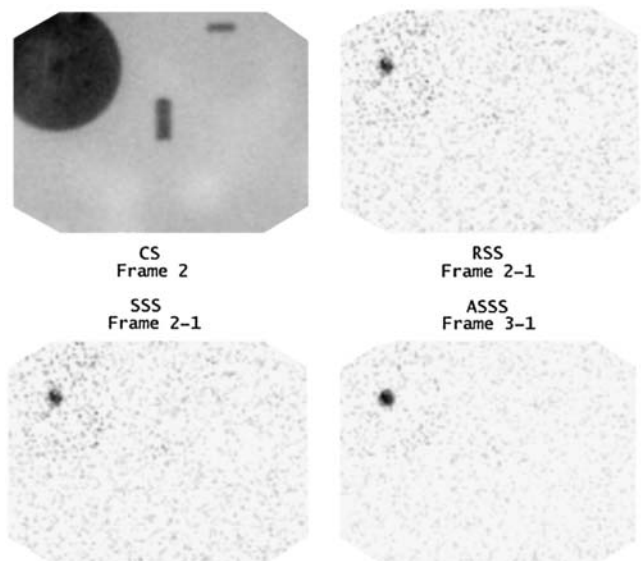


FIGURE 9. Bleed rate of $1.0 \text{ mL}\cdot\text{min}^{-1}$ with 5-min sampling interval. Lack of certainty exists for this liver bleed position in CS frame 2 (top left image). However, RSS (frame 2 – frame 1), SSS (frame 2 – frame 1), and ASSS (frame 3 – frame 1) provide “definitely present” outcome.

on a clinical basis because the complexity of the vascular compartment in the abdomen leaves few opportunities to easily identify a bleed in the presence of uniform background activity. The IVC results are more likely to simulate the superimposition of vascular structures experienced in the abdomen. Moreover, combining the results of CS and RSS improves test performance by 2% for the overall results and improves test performance for the IVC by 5%.

Interpretation of the results of this phantom study does require the consideration of several important points:

- Studies were truncated at 60 min; therefore, failure to identify the bleed does not mean that it would not have been detected had imaging continued past 60 min.
- Clinically, a bleed does not necessarily commence at the beginning of the acquisition, bleed at a uniform bleeding rate, or bleed for a protracted length of time.
- Clinically, a radiolabeled bleed may be diluted into a large bleed volume already resident in the bowel lumen from bleeding occurring before the completion of the $^{99\text{m}}\text{Tc}$ -labeled RBC labeling process.
- Clinically, a bleed may be more rapid than investigated in this study (e.g., $5 \text{ mL}\cdot\text{min}^{-1}$ or more) but may last only for a short duration. ASSS would provide benefits under these conditions.

One needs to consider that RSS was the same as ASSS at the more rapid bleeding rates by virtue of the fact that the same frame subtractions created the 2 files. This may not be the case clinically, because the actual bleed may commence at any time during the acquisition. Thus, a rapid bleeding rate might not be detected by RSS subtracting, for instance,

frame 50 from frame 1 because the bleed did not commence until frame 47. Detection would be subject to the effects of decay, changes in biodistribution over 50 min, subtraction of much higher background activity, and therefore a delay. The ASSS process would allow more accurate localization and, perhaps, earlier detection.

RSS improves the sensitivity in IVC hemorrhages, a result that suggests that clinically RSS may be useful in detecting some hemorrhages not revealed by CS because of a nonuniform background, an intense background, or high-count-density structure edges. Both RSS and ASSS also may have a role in increasing the certainty with which a diagnosis is made. Although CS should be the standard dataset, it should be supplemented by RSS to improve sensitivity and differentiation of possible false-positive and false-negative results. ASSS may provide a tool for more accurate localization.

CONCLUSION

A gastrointestinal tract hemorrhage study obtained with ^{99m}Tc -labeled RBCs has significantly higher background activity than does a study obtained with ^{99m}Tc -sulfur colloid, limiting the ability of the technique to confidently identify low-contrast lesions (delaying detection, increasing the minimum detectable bleed volume, and increasing the minimum detectable bleeding rate). An abnormal finding may be obscured completely. Despite this disadvantage, ^{99m}Tc -labeled RBCs are the radiopharmaceutical of choice because, among other reasons, they provide a significantly wider window of opportunity to image an active bleed than does ^{99m}Tc -sulfur colloid. The results of this phantom study provide evidence of a potential clinical role of subtraction scintigraphy in the evaluation of acute LGIH. Supplementing conventional datasets with RSS and ASSS may provide a useful tool that combines the advantages offered for lesion detectability by a high-contrast ^{99m}Tc -sulfur colloid study with the window of opportunity offered by ^{99m}Tc -labeled RBC scanning. Clinical evaluation of these processing techniques is warranted.

ACKNOWLEDGMENTS

This phantom study was supported by a Charles Sturt University Faculty of Health Studies seed grant. The authors would like to thank Matthew Haase for assistance during data collection.

REFERENCES

1. Peter DJ, Dougherty JM. Evaluation of the patient with gastrointestinal bleeding: an evidence based approach. *Emerg Med Clin North Am.* 1999;17:239–261.
2. Rosen RJ, Sanchez G. Angiographic diagnosis and management of gastrointestinal hemorrhage: current concepts. *Radiol Clin North Am.* 1994;32:951–967.
3. Billingham RP. The conundrum of lower gastrointestinal bleeding. *Surg Clin North Am.* 1997;77:241–252.

4. Maurer AH. Gastrointestinal bleeding. In: Murray IPC, Ell PJ, eds. *Nuclear Medicine in Clinical Diagnosis and Treatment.* 2nd ed., Vol. 1. London, U.K.: Churchill Livingstone; 1998:67–94.
5. Zeissman HA. The gastrointestinal tract. In: Harbert JC, Eckelman WC, Neumann RD, eds. *Nuclear Medicine: Diagnosis and Therapy.* New York, NY: Thieme Medical Publishers Inc.; 1996:585–650.
6. Anand AC, Patnaik PK, Bhalla VP, Chaudhary R, Saha A, Rana VS. Massive lower intestinal bleeding: a decade of experience. *Trop Gastroenterol.* 2001;22:131–134.
7. Cohen FS, Sohn N. Lower gastrointestinal bleeding. Available at: http://www.ssamed.com/pdf/presentation_lgb.pdf. Accessed September 29, 2004.
8. Enns R. Acute lower gastrointestinal bleeding: part 2. *Can J Gastroenterol.* 2001;15:517–521.
9. Vernava AM, Moore BA, Longo WE, Johnson FE. Lower gastrointestinal bleeding. *Dis Colon Rectum.* 1997;40:846–858.
10. Palmer EL, Scott JA, Strauss HW. *Practical Nuclear Medicine.* Philadelphia, PA: W.B. Saunders Co.; 1992.
11. DeMarkles MP, Murphy JR. Acute lower gastrointestinal bleeding. *Med Clin North Am.* 1993;77:1085–1100.
12. Longstreth GF. Epidemiology and outcome of patients hospitalized with acute lower gastrointestinal hemorrhage: a population based study. *Am J Gastroenterol.* 1997;92:419–424.
13. Coel M, Leung J. *Atlas of Nuclear Medicine.* Philadelphia, PA: W.B. Saunders Co.; 1996.
14. Dubovsky EV. Thyroid and parathyroid imaging. In: Baum S, RJ Campeau, Dubovsky EV, et al., eds. *Atlas of Nuclear Medicine Imaging.* 2nd ed. Norwalk, CT: Appleton & Lange; 1993:407–432.
15. Greenspan BS, Brown ML, Dillehay GL, et al. Procedure guideline for parathyroid scintigraphy. *J Nucl Med.* 1998;39:1111–1114.
16. Ford PV, Bartold SP, Fink-Bennett DM, et al. Procedure guideline for gastrointestinal bleeding and Meckel's diverticulum scintigraphy. *J Nucl Med.* 1999;40:1226–1232.
17. Zuckier LS. Acute gastrointestinal bleeding. *Semin Nucl Med.* 2003;33:297–311.
18. Gore RM, Tutton SM, Rattner Z, Maurer AH, Sparberg MS. Gastrointestinal hemorrhage. In: Gore RM, Levine MS, eds. *Textbook of Gastrointestinal Radiology.* 2nd ed., Vol. 2. Sydney, New South Wales, Australia: W.B. Saunders; 2000:2206–2227.
19. Kouris K, Abdel-Dayem HM, Awdeh M. Image subtraction in acute gastrointestinal bleeding studies using ^{99m}Tc -DTPA. *Nucl Med Commun.* 1985;6:717–722.
20. Seto H, Kageyama M, Wu YW, et al. Sequential subtraction scintigraphy with ^{99m}Tc -RBC for early detection of gastrointestinal bleeding. *Ann Nucl Med.* 1995;9:203–208.
21. Wu Y, Seto H, Shimizu M, et al. Sequential subtraction scintigraphy with ^{99m}Tc -RBC for the early detection of gastrointestinal bleeding and the calculation of bleeding rates: phantom and animal studies. *Nucl Med Commun.* 1997;18:129–138.
22. Wu Y, Seto H. Clinical value of sequential subtraction scintigraphy with ^{99m}Tc -RBC for gastrointestinal bleeding. *Chin Med J.* 2001;114:69–72.
23. International Commission on Radiological Protection. *ICRP Publication 23: Reference Man—Anatomical, Physiological and Metabolic Characteristics.* Philadelphia, PA: Elsevier; 1975.
24. Bland JM, Altman DG. Comparing two methods of clinical measurement: a personal history. *Int J Epidemiol.* 1995;24(suppl 1):S7–S14.
25. Alavi A, Dann RW, Baum S, et al. Scintigraphic detection of acute gastrointestinal bleeding. *Radiology.* 1977;124:753–756.
26. Thorne DA, Datz FL, Remley K, Christian PE. Bleeding rates necessary for detecting acute gastrointestinal bleeding with technetium- 99m -labeled red blood cells in an experimental model. *J Nucl Med.* 1987;28:514–520.
27. Datz FL, Thorne DA, Remley K, Christian PE. Determination of bleeding rates necessary for imaging acute gastrointestinal bleeding with ^{99m}Tc -labeled red blood cells [abstract]. *J Nucl Med.* 1986;27(suppl):956P.
28. Chandeysson PL, Hanson RJ, Watson CE, Henry GT. Minimum gastrointestinal bleeding rate detectable by abdominal scintigraphy [abstract]. *J Nucl Med.* 1983;24(suppl):97P.
29. Datz FL, Patch GG, Arias JM, Morton KA. *Nuclear Medicine: a Teaching File.* Sydney, New South Wales, Australia: Mosby; 1992.
30. Hassan F, Naddaf S, Al-Enizi E, Elgazzar AH. Gastrointestinal tract. In: Elgazzar AH, ed. *The Pathophysiological Basis of Nuclear Medicine.* New York, NY: Springer; 2001:284–293.
31. Kostamo KL. Evaluation of gastrointestinal bleeding by nuclear medicine techniques. In: Henkin RE, Boles MA, Dillehay GL, et al., eds. *Nuclear Medicine.* Sydney, New South Wales, Australia: Mosby; 1996:1016–1022.